Influence of ultraviolet wavelengths on kinetics and selectivity for N-gases during TiO₂ photocatalytic reduction of nitrate

Heather O'Neal Tugaoen[a,b,*], Pierre Herckes[c], Kiril Hristovski[d], Paul Westerhoff[a]

[a] School of Sustainable Engineering and the Built Environment, Arizona State University, 660 S. College Avenue, Tempe, AZ 85287, United States
[b] College of Science, Engineering, and Technology, Grand Canyon University, 3300 W. Camelback Road, Phoenix, AZ 85017, United States
[c] School of Molecular Sciences, Arizona State University, 875 S. Palm Walk, Tempe, AZ 85287, United States
[d] The Polytechnic School, Arizona State University, 7171 E Sonoran Arroyo Mall, Mesa, AZ 85212, United States

ARTICLE INFO

ABSTRACT

For drinking water applications, photocatalytic reduction processes beneficially transform aqueous nitrate to innocuous nitrogen gases (N-gases) but can produce nitrite and ammonia as undesirable aqueous by-products. We hypothesize that by-product selectivity is a function of light source and photon fluence dose, such that discrete wavelengths can increase yield of desirable N-gases. Experiments performed under different wavelength irradiation (ultraviolet- [UV] A, B, C) reduced nitrate in water to differing extents based on pH over the range of 1–8 or the presence of soluble organic electron donors. At an equivalent photon fluence dose, the most rapid nitrate loss in acidic solutions occurred using a combination of three UV-light emitting diodes (285 nm, 300 nm, 365 nm) closely followed by a polychromatic medium pressure UV lamp. A polychromatic xenon light source was least effective in reducing nitrate. Nitrite is an important intermediate during photocatalytic reduction of nitrate. Nitrite absorbs 330–380 nm light with high quantum efficiency. Thus, polychromatic or monochromatic light sources with strong UV-A emission more rapidly convert nitrite to by-products than UV-C monochromatic light sources. Nitrous acid (HONO) has a higher molar absorptivity (ε) and quantum efficiency than nitrite ion ($pK_a = 3.39$) around 350–370 nm. Selectivity towards N-gases is bifurcated at the nitrite intermediate and is strongly influenced by direct photolysis instead of photocatalytic reduction. Thus, the selectivity of by-products can be controlled by delivering light in the 350–370 nm wavelength range, where it enables photocatalytic processes to rapidly initiate NO_3^- reduction and delivers photons for direct photolysis of HONO.
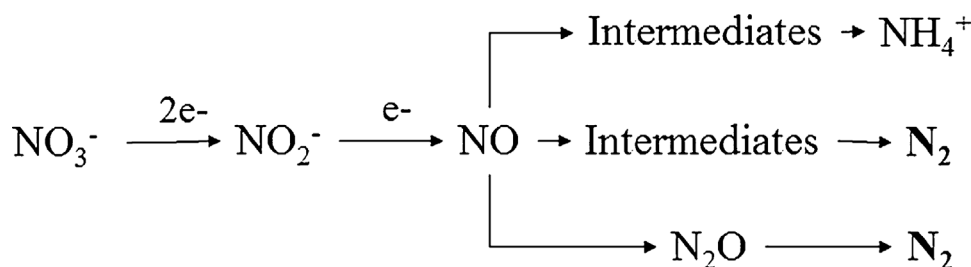
1. Introduction

Nitrate contamination in drinking water is globally pervasive, affecting over 24 million people in the United States alone, with concentrations above the 10 mg-N/L maximum contaminant level (MCL) set by the United States Environmental Protection Agency [1]. The National Academy of Engineering has listed management of the nitrogen cycle and provision of clean water as two of its top twelve grand challenges [2]. Dealing with ubiquitous nitrate contamination requires transformation of fixed nitrogen in the aqueous phase to innocuous gaseous products (e.g., N₂). Accepted technologies for nitrate removal from drinking water include ion-exchange and reverse osmosis, but both of those yield product waters (i.e., brines) containing concentrated nitrate instead of transforming nitrate into N-gases. Biological denitrification is excellent for wastewater treatment, but managing organic or hydrogen electron donors, bacteria populations, release of soluble organics, and rapid start up and shut down of systems can be difficult

for small drinking water systems [3]. Physical-chemical treatment processes are more feasible to implement at small system scale because they are less operationally intensive and are more reliable than biological processes for nitrate reduction. Emerging solutions for nitrate reduction are photocatalysis [4,5], catalytic hydrogen reduction [6–11], and electrochemical reduction [12–14], whereby nitrate is terminally reduced to innocuous N-gases (e.g., N₂) and minimal aqueous ammonium. Herein, we focus on photocatalysis for reduction of nitrate because it uses environmentally benign photocatalysts, uses efficient photonic light sources, and can completely reduce nitrate to innocuous N-gases (e.g., N₂).

Photocatalytic reduction can treat nitrate in drinking water directly or treat ion exchange brines [15] to produce both aqueous and gaseous constituents with varying implications and toxicity [16–18]. A primary challenge for photocatalysis is to avoid ammonium production, which occurs readily at neutral pH [19]. Aqueous ammonia production is undesirable in drinking waters because it exerts a chlorine demand

Scheme 1. Conceptual sequence for nitrate reduction to desirable nitrogen gas (N_2) and undesirable ammonium ion.

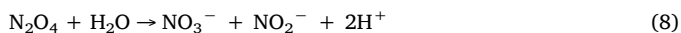upon disinfection in water distribution systems. The preference is a sparingly soluble non-ammonia N-gas by-product (e.g., N_2, NO_x). Selectivity toward non-ammonia N-gases may be further controlled in photocatalytic systems via adjustment of experimental and reactor parameters [20].

Previous studies have focused efforts on managing by-product selectivity through manipulation of experimental conditions, including: pH [21,22], alkalinity [22,23], sacrificial electron donor [5,21], salinity [15,24,25], and photocatalyst [5,15,21–23,26–46]. The literature shows N-gases by-product formation ranging from > 80% to < 10%. These differences in selectivity emerge from aforementioned experimental solution conditions (pH [21,22], presence of external electron donors [5,21], or photocatalyst properties [39,41,43,44,46]). Common experimental conditions [5,21,22,38] are 1 g/L of photocatalyst and 40 mM HCOOH to (1) satisfy low-pH conditions and (2) serve as a sacrificial hole scavenger. Acidic conditions are preferred for nitrate reduction to N-gases, with HCOOH yielding the best kinetics and selectivity at pH $\approx$ 2.5 [21]. Recent works have identified $CO_2 \cdot^-$, a product of HCOOH oxidation [47–49], as a primary photocatalytic mechanism for reduction of nitrate to nitrite in lieu of the conduction band electron due to its thermodynamic feasibility [5,18]. Near the pKa of 3.39, nitrous acid (HNO_2, HONO; Eq. (1)) forms, which is more photoactive in the mid 300 nm range (quantum yield, $\Phi_{280\text{-}385nm}$ = 0.35–0.45 [50–52]) than nitrite ion ($\Phi_{280\text{-}385nm}$ = 0.025–0.15 [53]). However, this photolytic reaction is predominantly circular, yielding NO_2^- (Eqs. (3)–(5)).

$$NO_2^- + H^+ \leftrightharpoons HONO \qquad pK_a = 3.39 \qquad (1)$$

$$NO_3^- + H^+ \leftrightharpoons HNO_3 \qquad pK_a < 1 \qquad (2)$$

$$HONO + h\nu \to NO\cdot + OH\cdot \qquad (3)$$

$$NO\cdot + NO_2\cdot \to N_2O_3 \qquad (4)$$

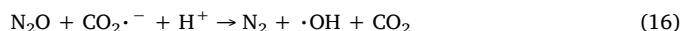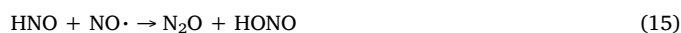$$N_2O_3 + H_2O \to 2NO_2^- + 2H^+ \qquad (5)$$
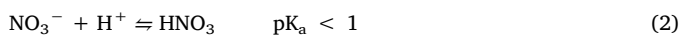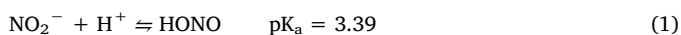
Due to the complex photochemistry, a parallel reaction reforming NO_3^- and NO_2^- is likely co-occurring via Eqs. (6)–(8) (which may contribute to oxidation of NO_2^- in situ):

$$NO\cdot + NO\cdot \to N_2O_2 \qquad (6)$$

$$N_2O_2 + O_2 \to N_2O_4 \qquad (7)$$

$$N_2O_4 + H_2O \to NO_3^- + NO_2^- + 2H^+ \qquad (8)$$

Photocatalysis with pristine titanium dioxide (TiO_2) does not produce e_{cb}^- of sufficient energy to initiate nitrate reduction to nitrite or reduce all intermediates to N-gases [20]. Formic acid oxidation occurs directly via h_{vb}^+ to yield carboxyl radical ($CO_2 \cdot^-$) according to Eqs. (9) and (10) [47–49]:

$$Semiconductor + h\nu \to h_{vb}^+ + e_{cb}^- \qquad (9)$$

$$HCOO^- + h_{vb}^+ \to H^+ + CO_2\cdot^- \qquad (10)$$

Combining photocatalysis with photolysis, reactions proceed that yield gaseous products (Eqs. (11)–(16) [53,54] will occur:

$$HONO + e^- \to NO\cdot + OH^- \qquad (11)$$

$$NO\cdot + e^- \to NO^- \qquad (12)$$

$$NO^- + H^+ \leftrightarrow HNO \qquad (13)$$

$$2HNO \to N_2O + H_2O \qquad (14)$$

$$HNO + NO\cdot \to N_2O + HONO \qquad (15)$$

$$N_2O + CO_2\cdot^- + H^+ \to N_2 + \cdot OH + CO_2 \qquad (16)$$

Targeting HONO/HNO as key intermediates for evolution of N-gases offers a method to minimize ammonium production via transformative processes yielding N-gases (Eqs. (11)–(16)). TiO_2 photocatalysis has been postulated in the literature to include nitrate reduction reactions to largely unsubstantiated intermediate constituents as articulated in Scheme 1. Common products include aqueous NO_2^- or NH_4^+, or gaseous species such as N_2 (most common) NO [55], or N_xO_y [56] which are aggregated as N-gases. Photocatalysis reduces nitrate to nitrite [53] via a stepwise two-electron transfer. Both photocatalytic and photolytic pathways are more relevant for nitrite reduction to ammonia or N-gases, but to date their impacts have only been investigated separately.

Light sources emit different wavelengths, and the role of light constitutes an excitement of electrons within photocatalysts in parallel to photolysis of aqueous nitrogen species. Each aqueous nitrogen species absorbs photons of different wavelengths corresponding to different photolytic quantum yields. For photocatalysis, the bandgap energy must be exceeded to produce electrons for reduction. Likewise, hole scavengers may undergo photolytic processes under short-wavelength irradiation, yielding oxidation products such as the $CO_2 \cdot^-$ radical in the case of HCOOH. Thus, incident wavelengths should play a significant role in reduction kinetics and selectivity, with arbitrary selections leading to energetic/photonic inefficiency and ammonium production. Although many studies report nitrate loss and by-product formation as a function of irradiation duration, they often do not provide the irradiation spectrum or light intensity in the reactor, thereby complicating direct comparisons between studies [5,22,39–41,44,57]. Photon (and energy) fluence values can be used to directly compare efficiency across irradiance sources of varied wavelength and intensity and are utilized herein to provide a normalized comparison of seemingly disparate light sources.

Photocatalytic nitrate reduction has been explored using a TiO_2 or metal/metal oxide-TiO_2 photocatalyst under irradiation by xenon lamps or medium pressure or high pressure mercury lamps [46,53]. The highest selectivity toward N-gases under these irradiation conditions utilize TiO_2, TiO_2/Ag, or TiO_2/Cu in acidic solutions containing HCOOH. A detailed literature review on photolysis and photocatalysis of nitrate is provided elsewhere [20]. From this review, we hypothesize that nitrate photocatalytic degradation and by-product selectivity is a function of light source and photon fluence dose at key wavelengths and that particular discrete wavelengths will predominantly yield N-gases through a combined photocatalytic/photolytic mechanism. To test this hypothesis, multiple light sources with different emission spectra were used to address the following objectives: (1) compare absorbance spectra of aqueous N-species and TiO_2 photocatalyst against emission spectra of polychromatic light sources; (2) demonstrate photocatalytic reduction of nitrate in acidic solutions with an external

aqueous electron donor using polychromatic light sources; (3) quantify how wavelength filters coupled with polychromatic light sources change photocatalytic nitrate reduction products; (4) compare the effects of polychromatic light sources and discrete irradiation wavelengths (using light emitting diode [LED] sources) on photocatalytic reduction of aqueous nitrate and nitrite; and (5) postulate mechanisms for indirect photocatalytic and direct photolytic pathways for reduction of aqueous nitrate to N-gases, identifying nitrite as a critical intermediate and point of bifurcation in selectivity outcomes. An assessment of the combined effect of photocatalytis and photolysis from a light-delivery perspective (changing incident wavelengths) had not been conducted for the enhanced removal of aqueous nitrate and selectivity toward N-gases prior to this work.

2. Methodology

2.1. Absorption spectra determination

Aqueous absorption spectra were measured using UV/vis spectroscopy (DR5000, HACH) and calculating molar absorptivities according to the Beer-Lambert Law. Quantum efficiencies were compiled from the literature to compare expected photolytic yields of aqueous nitrogen species. Diffuse reflectance spectra of solid photocatalyst samples were measured using a Lambda 18 (Perkin Elmer, USA) with a 150 mm integrating sphere to determine the absorption spectrum of the photocatalyst.

To quantify the spectral output of the polychromatic light sources, irradiance was measured using a fiber optic spectrometer with cosine corrector (Avantes AvaSpec 2048). Multiple locations were measured in the reactors to provide average irradiance values. Fluence dose (mJ/cm^2) and photon fluence dose (photon/cm^2) were calculated [58,59] to represent (1) the full spectrum of light emitted by the source and (2) partial spectrum based on the assumption that only wavelengths available for P90 (TiO$_2$) bandgap excitation (ultraviolet, $\lambda \leq 388$ nm) were experimentally relevant.

2.2. Determining photocatalytic nitrogen reduction

Commercially available titanium dioxide (Evonik) was obtained as a powder (P90) and used as received. P90 contains anatase (86%, 12 nm) and rutile (14%, 18 nm) crystal phases and has a surface area of 104 m^2/g [38]. P90 has a higher nitrate reduction rate compared to P25 [38]. Sodium nitrate (NaNO$_3$, 99% EMD Millipore) and sodium nitrite (NaNO$_2$, 97% Sigma) were the nitrate and nitrite source, respectively. Formic acid (HCOOH, 98% Fluka) was the sacrificial electron donor (hole scavenger) in experiments where indicated. All experiments were performed in 18.2 MΩ-cm Nanopure® water with no buffering.

Most experimental conditions were consistent with prior work [21,22]. In brief, the pH was 2.5, and the water matrix contained 100 mg-NO$_3^-$-N/L (7.14 mM), 40 mM HCOOH, and 1 g/L P90. Parallel experiments were conducted with 100 mg-NO$_2^-$-N/L (7.14 mM) instead of nitrate as noted. In all experiments, 30 min dark adsorption preceded illumination to determine non-photocatalytic removal of nitrogen due to adsorption. In all reactors, magnetic stirring was employed to maintain photocatalyst suspension.

Samples were collected from the reactors over time and filtered (0.2 μm nylon membrane filters, Pall). Cumulative sample volumes collected from the reactors were < 10% of aqueous phase reactor volume to preserve experimental conditions. Samples were stored in amber glass vials in dark conditions for analysis within 48 h. Aqueous concentrations of nitrate, nitrite, and ammonium were analyzed (EPA Method 300.0, ASTM Standard Method D6919) using a dual anion/cation ion chromatography instrument (ICS-5000, Dionex). Results are reported as total nitrogen reduction (TNR), which we define using concentrations [mg-N/L] of initial (0) and final (f) aqueous constituents according to Eq. (17):

$$TNR = 100 * \left(1 - \frac{[[NO_3^-] + [NO_2^-] + [NH_4^+]]_f}{[[NO_3^-] + [NO_2^-] + [NH_4^+]]_o} \right) \tag{17}$$

The selectivity to gaseous nitrogen species was based on the difference of initial (0) and final (f) aqueous constituents and was calculated according to Eq. (18):

$$S(N_{gases}) = \frac{[NO_3^-]_o - [NO_3^-]_f - [NO_2^-]_f - [NH_4^+]_f}{[NO_3^-]_o - [NO_3^-]_f} \tag{18}$$

To study reactivity of an important intermediate species, experiments were conducted starting with nitrite instead of nitrate. Nitrite or HONO reduction was investigated using either broad-wavelength or discrete wavelength irradiation to elucidate the reaction bifurcation mechanism that produces either aqueous ammonium or N-gases. TNR was used to quantify nitrogen removal from the aqueous phase. Dark adsorption testing at pH 2.5 induced non-photonic HONO oxidation, which likely contributed to the observed nitrate concentrations (< 8%).

2.3. Photocatalytic light sources and reactors

Experiments using a 450 W medium pressure mercury lamp (UV: 100 mW/cm^2) were conducted in a double-walled quartz immersed-lamp photoreactor (200 mL; Ace Glass power supply, 7830-60; Ace Glass, 78-25-34; Hanovia PC 451.050) with external cooling water to maintain constant temperature (25 °C). A borosilicate sleeve surrounded the lamp to filter out wavelengths lower than 280 nm and eliminate direct photolysis of nitrate or formate.

Experiments using a 450 W Xe-arc lamp (300 mW/cm^2, 66924-450XV-R1, Newport) were performed in a 150 mL reactor, which was separated from the lamp by a quartz window (d = 7 cm) and water filter to eliminate infrared irradiation and reactor heating from the irradiation source. For some experiments, an ultraviolet cutoff filter (Newport, 90017074) selectively blocked wavelengths between 280 nm and 450 nm to eliminate UV-A (315 nm to 400 nm) and UV-B (280 nm to 315 nm) irradiation to only transmit 240 nm–280 nm for isolated UV-C testing. Xenon lamp experiments were performed to compare results of broad-wavelength irradiation to the polychromatic spectrum of the medium pressure mercury lamp.

Experiments at 285, 300, and/or 365 nm were performed in a Petri dish reactor (40 mL) using an LED collimated beam light source (AquiSense PearlBeam custom UV-LEDs) with incorporated heat sink, fan, and quartz viewing lens. Light was collimated (13 cm column, 10 cm diameter) to ensure a uniform LED array across the 10 cm Petri dish diameter. Illumination was delivered using the LEDs individually and in varied combination: 285 nm, 300 nm, or 365 nm alone; 285 nm and 300 nm combined; or 285 nm, 300 nm, and 365 nm combined. These specific wavelengths were chosen based on a comprehensive survey of the literature (quantum yields, etc.) [20] and prior experimental work indicating high NO$_3^-$/NO$_2^-$ reduction with high N-gas selectivity. LED light source experiments investigated discrete wavelength polychromatic irradiation in comparison to more broadly emitting medium pressure Hg and Xe lamps.

3. Results and discussion

3.1. Comparing light source emission spectra with absorptivity spectra of N-species and TiO$_2$

Among the ionic aqueous nitrogen species, nitrite has the highest molar absorptivity (ε) in the 280–400 nm range (Fig. 1). Between 350 and 370 nm, HONO has a maximum ε (~ 40 M^{-1} cm^{-1}) approximately twice that of NO$_2^-$. Nitrate has a maximum ε at 300 nm and very low ε between 350 and 380 nm. Ammonium ion (NH$_4^+$) and hydroxylamine (H$_3$NO) have negligible absorbance (ε < 0.5 M^{-1} cm^{-1}) in the UV range. Higher absorptivity does not directly correspond to higher

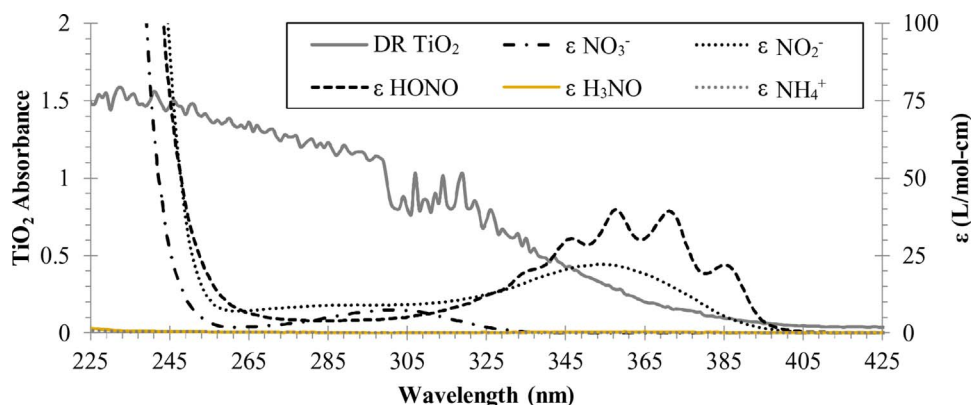photolytic activity because of the variable quantum yields, as described by Mack and Bolton [53]. Thus, depending on the light source used and its particular irradiation emission spectrum, different direct photolysis reactions may occur, both of primary species and aqueous or adsorbed intermediates.

Fig. 2 illustrates the ultraviolet spectral output of: (a) the polychromatic medium pressure mercury lamp; (b) xenon lamp filtered to exclude wavelengths between 280 and 450; (c) xenon lamp allowing all wavelengths (i.e., not filtered); and (d) UV-LED irradiation source at 285, 300, and 365 nm. Comparing the absorbance spectra in Fig. 1 with the emission spectra in Fig. 2 suggests photons from the 365 nm LED would be absorbed more by HONO than NO$_2^-$, and little absorbance would occur by NO$_3^-$ or other aqueous N-species. Light with $\lambda \approx 295$ nm that is delivered into the solution would be absorbed by NO$_2^-$, NO$_3^-$, and HONO. At 295 nm and throughout the ultraviolet spectrum, these species will undergo direct photolysis to different extents due to their varied quantum yields [53].

Fig. 1 also illustrates the diffuse reflectance spectra for TiO$_2$. In suspended slurry, TiO$_2$ scatters or absorbs light below 400 nm. This scattering reduces photon transmittance into solution and limits direct photolysis of aqueous N-species to the portions of solution that are closest to the light source. As such, the emission spectra of the light source and the interfacial area between the lamp source and water both influence the reactivity due to direct photolysis and the TiO$_2$ catalyzed areas. Overall, a weaker photolytic and more dominant photocatalytic response would be expected for slurry photocatalysis. P90, with a bandgap of 3.2 eV [38], absorbs light below 390 nm as calculated with the Kubelka-Monk Equation. As described by Planck-Einstein relationship, each wavelength corresponds to a different energy. Photons with lower energy ($\lambda > 390$ nm) are thereby not relevant for production of

aqueous electrons associated with TiO$_2$. Further, photons with $\lambda > 390$ nm are also not relevant for direct photolysis reactions with aqueous N-species. Thus, on an energy basis, only photons with $\lambda < 390$ nm are considered effective for nitrate photocatalysis and/or photolysis and are tabulated as such for photon fluence values reported in this work.

3.2. Nitrate removal during photocatalysis with different polychromatic light sources

To assess the variability of nitrate reduction kinetics and by-product selectivity across irradiation sources, three light sources and reactor configurations delivered varied-wavelength photons for photocatalytic reduction of nitrate. Prior experiments using medium pressure mercury lamp photocatalysis with TiO$_2$ show nitrate reduction [5,22,38,46], but new insights may be gained through assessing the system's photonic efficiency. Fig. 3 shows nitrate concentrations decreasing over irradiation time with low production of nitrite or ammonia for the medium pressure Hg light source emitting wavelengths longer than 240 nm in the presence of TiO$_2$ and an external electron donor (HCOOH). Nitrite formed as a detected intermediate, accounting for a maximum of 20% of the nitrogen after 28 min of irradiation, though its reduction proceeds at significantly higher rate than nitrate [20]. The net loss of aqueous N-containing species was consistent with evolution of volatile N-gases [18,22,56]. Control experiments in the dark showed no nitrate removal.

Rather than evaluating concentration changes based on reaction time, reaction kinetics are also plotted as a function of photon fluence dose (photons/cm^2) and fluence dose (mJ/cm^2) to facilitate comparisons between irradiation sources. Energy-based fluence has been used
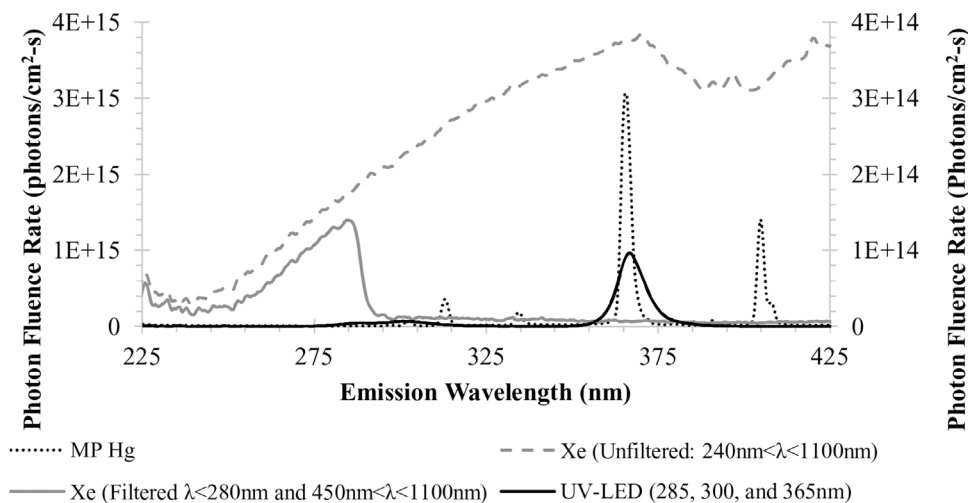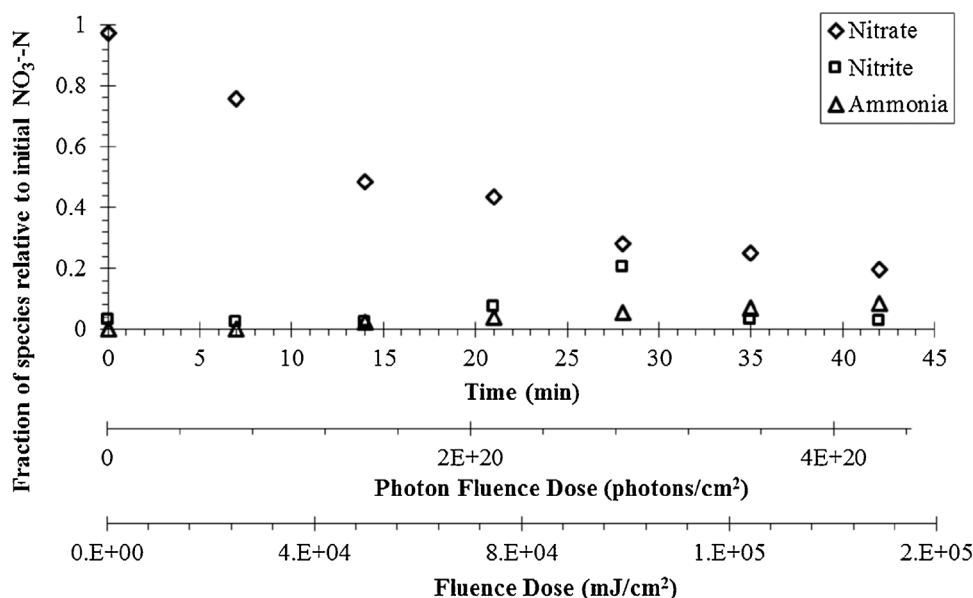
Fig. 3. NO_3^- photocatalytic reduction and by-product formation (nitrite and ammonia) under medium pressure mercury irradiation with 1 g/L TiO_2 (P90) and 40 mM HCOOH (pH = 2.51 ± 0.05).

to assess microbial inactivation by UV light [60,61], demonstrating wavelength-dependent outcomes [62] in UV disinfection performance studies. When nitrate reduction is observed experimentally, the irradiation source generates photons at wavelengths that exceed bandgap energy or induce photolytic response from aqueous N-species. Because N-species may undergo direct photolysis at different wavelengths plus indirect reduction on photo-excited TiO_2, photon fluence facilitates comparisons across the various wavelength sources when quantifying N-reduction efficiency.

Table 1 summarizes experimental data for the same initial aqueous conditions as illustrated in Fig. 3 but under irradiation with a xenon lamp. Xenon lamp irradiation can yield both photocatalytic and direct photolytic response for nitrate reduction due to its photon production at $\lambda < 290$ nm. For both wavelength-filtered and unfiltered xenon irradiation, negligible ammonium or nitrite formed, indicating complete reduction to N-gases. Irradiation of a nitrate solution with the unfiltered xenon source achieved double the nitrate reduction (46%) after an applied photon fluence dose of 4.8×10^{20} photons/cm^2 with 1 g/L TiO_2 compared against 21% nitrate reduction in the absence of TiO_2 after the same photon fluence dose. This implies that direct photolysis of nitrate occurs for 240–400 nm xenon irradiation, but a higher net removal of nitrogen (as N) occurs via combined direct photolysis and photocatalysis in the presence of TiO_2. UV-C only ($\lambda < 280$ nm) irradiation using the xenon source achieved 20% nitrate reduction during direct photolysis (with HCOOH) but less than 14% nitrate reduction

during photocatalysis (1 g/L TiO_2) at a photon fluence dose of $\sim 5.5 \times 10^{19}$ photons/cm^2, indicating higher efficiency of nitrate photolysis than photocatalysis at wavelengths less than 280 nm. Nitrate undergoes direct photolysis at wavelengths less than 290 nm [63–65], which causes photolytic processes to dominate the mechanisms for its reduction in the UV-C region. In contrast, TiO_2 has broad absorption throughout the UV-A to UV-C range, allowing for photocatalysis to co-occur with photolysis when the xenon lamp is used without the 280–450 nm wavelength filter (transmits 240–280 nm and $\lambda > 450$ nm).

Experiments were conducted using 285, 300, and 365 nm LEDs operating simultaneously under identical initial aqueous conditions as those in Fig. 3. This LED configuration outperforms the other light sources on a reduction per-photon or per-mJ basis (Fig. 4), though it requires a longer time to achieve nitrate reduction due to the low photon fluence rate of the LEDs. The maximum achieved photon fluence dose was 2.3×10^{19} photons/cm^2 for the LED, which is 2.4 times lower than the xenon lamp experiment (Table 1) and 18 times lower than the mercury lamp due to the scale of the system employed. At an equivalent 0.23×10^{20} photon/cm^2 photon fluence dose in the mercury lamp experiment, $\sim$9% of nitrate reduction was achieved compared with 15% for polychromatic LEDs. On a time-basis, these two polychromatic photoreactors appear to perform quite differently, but the energetic and photonic efficiency are similar. This result should allow for transitioning from Hg-based irradiation sources to more

Table 1

Reduction of Nitrate or Nitrite (as NO_2^- 0 mM HCOOH, pH = 5.5; as HONO 40 mM HCOOH, pH = 2.5) under Wavelength Filtered or Unfiltered Xenon Lamp Irradiation (UV Wavelengths Emitted: 240–280 nm or 240–400 nm, respectively). Initial concentrations for all cases were 100 mg-N/L.

| Initial N-Species	Effective Irradiation Wavelengths (UV-only)	Applied Fluence Dose (mJ/cm^2)	Applied Photon Fluence Dose (photons/cm^2)	P90 Dose (g/L)	Initial Formic Acid (mM)	% Reduction of Total Aqueous Nitrogen
NO_3^-	240–400	1.70×10^8	4.83×10^{20}	0	0	0.5
NO_3^-	240–400	1.70×10^8	4.83×10^{20}	0	40	21.2
NO_3^-	240–400	1.70×10^8	4.83×10^{20}	1	40	46.2
NO_2^-	240–400	1.70×10^8	4.83×10^{20}	0	0	9.4
NO_2^-	240–400	1.70×10^8	4.83×10^{20}	0	40	83.2
NO_2^-	240–400	1.70×10^8	4.83×10^{20}	1	40	99.9
NO_3^-	240–280	2.30×10^7	5.49×10^{19}	0	0	5.0
NO_3^-	240–280	2.30×10^7	5.49×10^{19}	0	40	20.1
NO_3^-	240–280	2.30×10^7	5.49×10^{19}	1	40	13.9
NO_2^-	240–280	2.30×10^7	5.49×10^{19}	0	0	3.8
NO_2^-	240–280	2.30×10^7	5.49×10^{19}	0	40	82.1
NO_2^-	240–280	2.30×10^7	5.49×10^{19}	1	40	84.3
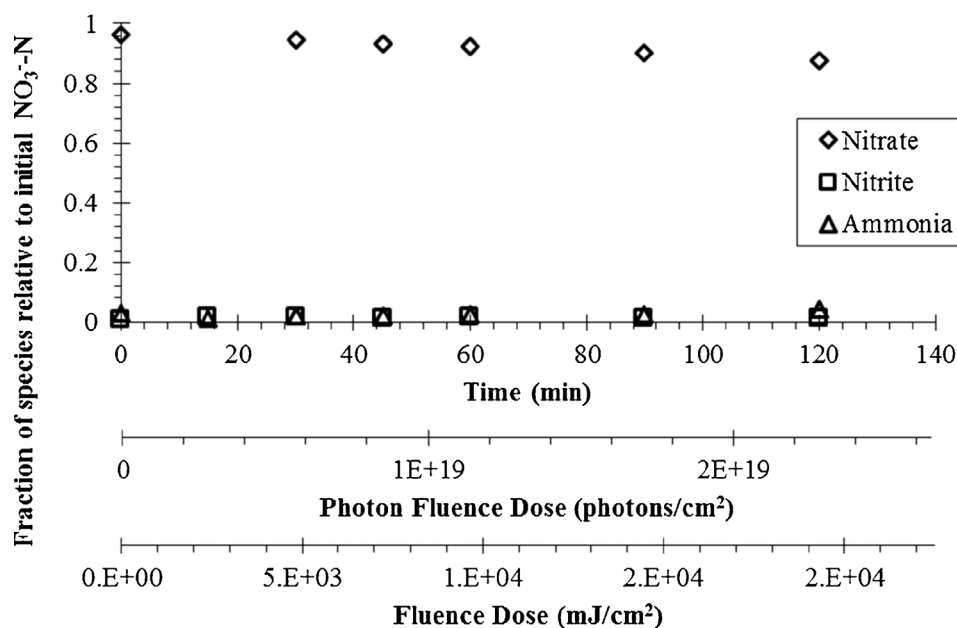
Fig. 4. NO_3^- photocatalytic reduction and by-product formation (nitrite and ammonia) under 285, 300, 365 nm UV-LED irradiation with 1 g/L TiO_2 (P90) and 40 mM HCOOH (pH = 2.51 ± 0.05).

innocuous and compact LED systems where appropriate (e.g., small systems, point of use facilities) when high output LEDs become available. These experiments show the need to select the appropriate units of fluence to evaluate nitrate photocatalytic reduction; the preferred units consider wavelengths in the photoactive region (200–400 nm) for TiO_2 and aqueous N-species.

3.3. Kinetics and selectivity of by-products during nitrate photocatalysis

Tables 2 and S1 show that photocatalytic reduction of nitrate yields the following final conversion of NO_3^- and selectivity to N-gases S (N_{gases}) for the medium pressure Hg, Xe (240–280 nm), Xe (240–400 nm), and UV-LEDs (285, 300, 365 nm): 78% with 89% S (N_{gases}), 14% with 100% S(N_{gases}), 46.2% with 100% S(N_{gases}), and 10% with 82% S(N_{gases}), respectively. Based on these values alone, comparison would yield significantly different key insights than further examination based on photon fluence and energetic kinetic rates. Changes in nitrate removal throughout an experiment were fitted by pseudo-first order kinetics with respect to time, photon fluence dose, or fluence dose. Fig. 5 illustrates an example of photocatalytic nitrate reduction data for the medium pressure Hg lamp fitted with pseudo-first order kinetics and reporting of rate constants using three corresponding units for kinetics. Tables 2 and S1 show the rate constants (k) expressed in three different forms—time (sec^{-1}), photon fluence dose (photon/cm^2)$^{-1}$, and fluence dose (mJ/cm^2)$^{-1}$—for all irradiance sources. These tables also contain values for aqueous and gaseous selectivity for polychromatic experiments.

Fig. 6 shows half-lives of nitrate reduction computed from the pseudo-first order rate constants ($t_{1/2} = \frac{\ln 2}{k}$) with respect to
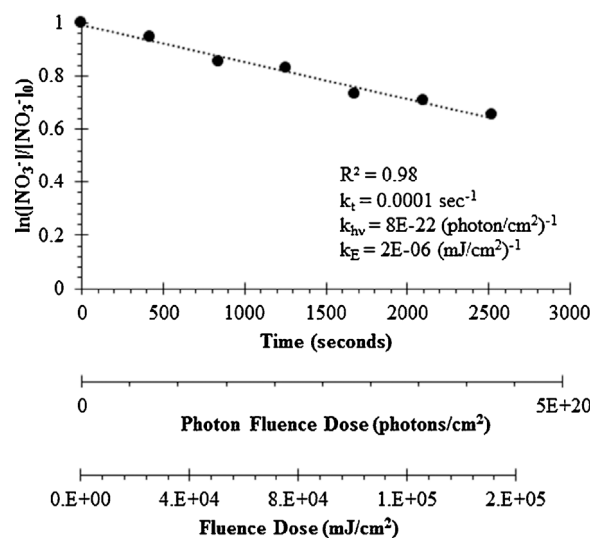

Fig. 5. Pseudo-first order nitrate removal kinetics using medium pressure lamp with 1 g/L TiO_2 (P90), and 40 mM HCOOH (pH = 2.5 ± 0.05) with respect to time, photons, and energy.

experimental time, photon fluence dose, and fluence dose. Shorter $t_{1/2}$ values occurred for medium pressure Hg irradiation on a time-basis or LED irradiation on a photon- and energy-basis. Accounting for all incident wavelengths (200–1100 nm), the UV-LED combination had the shortest half-life (i.e., best performance) at 1.08×10^{20} photons/cm^2 (0.56×10^5 mJ/cm^2) compared to 1.81×10^{20} photons/cm^2

Table 2
Summary of Kinetic Data for NO_3^- Reduction Experiments under Varied Irradiance Conditions[a].

Light Source	Final% NO_3^-–N Reduction	k_{time} (10^{-5} s^{-1})	k_{light} (10^{-22} cm^2/photon)	k_{energy} (10^{-6} cm^2/ mJ)	TNR (% N) Removed	Selectivity (%)		
						N_g	NO_2^-	NH_4^+
Medium Pressure Hg	77.96	64.5	38.3	10.9	69.1	89	0	11
Xe (240–280 nm)	13.9	2.31	0.18	0.065	13.9	100	0	0
Xe (240–400 nm)	46.2	17.3	1.49	0.581	30.6	100	0	0
UV-LED (285, 300, 365 nm)	9.76	1.60	63.9	12.3	9.48	82	2	16

[a] All experiments in Table 2 were conducted with initial NO_3^--N concentration of 100 mg-N/L, 40 mM HCOOH, and 1 g/L P90 TiO_2 catalyst. Wavelength data include all produced wavelengths (200–1100 nm).
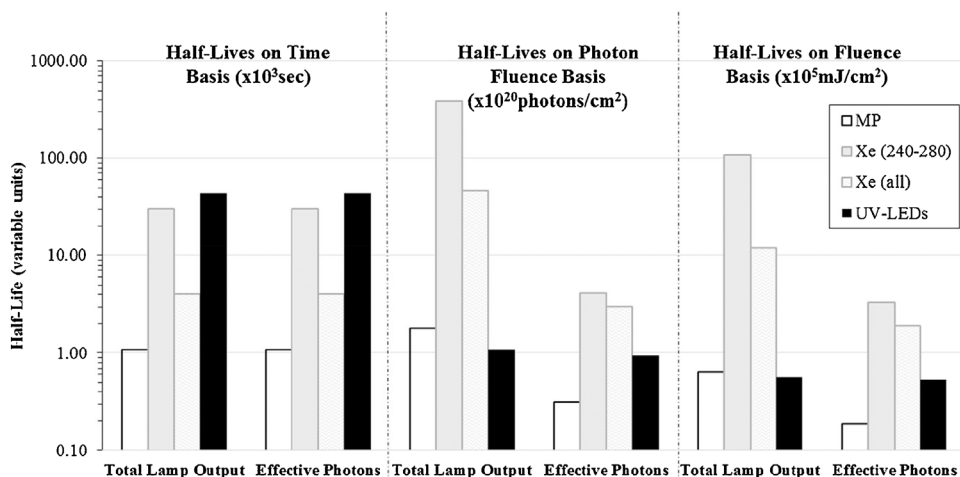
Fig. 6. Half-life of NO_3^- reduction kinetics with respect to time ($x10^3$ s), photons ($x10^{20}$ photons/cm²), and energy ($x10^5$mJ/cm²) for medium pressure lamp, xenon lamp with UV-filter to include 240–280 nm only or xenon lamp without UV filter to include all wavelengths, and 285, 300, 365 nm UV-LED combination array. Experimental parameters: 100 mg-NO_3-N/L, 1 g/L P90, 40 mM HCOOH (pH = 2.5 ± 0.05). Total lamp output considers all wavelengths incident to reactor, and effective photons delineates wavelengths (< 380 nm) absorbable by TiO_2.

$(0.63 \times 10^5$ mJ/cm²) for the medium pressure Hg lamp. Due to the broad-band irradiation from the xenon lamp, half-life for reduction of nitrate for both UVC and UVA-UVC irradiation was $> 10 \times$ higher than that of the medium pressure or LED sources. This is because much of the energy used to produce photons for the medium pressure Hg and xenon lamps is effectively wasted in a TiO_2-based photocatalytic system because UV wavelengths are required for excitation.

Differences in nitrate removal and product selectivity between irradiation sources indicates key wavelengths dominated the process of nitrate reduction to N-gases. In broad-spectrum irradiance conditions, a photonic saturation occurred, where excess light merely lowered efficiency rather than promoting nitrate reduction. A secondary effect was the known mass-transfer limitation of nitrate in photocatalytic systems. This limitation further induces the photonic saturation while photocatalyst reactive sites may undergo excitation and recombination prior to contact with aqueous nitrogen species [66].

3.4. Photocatalysis and direct photolysis of HONO and NO_2^-

Nitrite photolysis (pH = 5.5) with a xenon lamp led to 9% TNR for the 240–400 nm range and only 4% TNR for the 240–280 nm range (Table 1) at a photon fluence dose of 4.83×10^{20} photon/cm² and 5.49×10^{19} photon/cm², respectively. In contrast, over the same wavelength ranges, the effect of lowering pH to conjugate NO_2^- to HONO allowed for HONO photolysis (pH = 2.5) and more removal compared to NO_2^-: 83% TNR (240–400 nm) and 82% TNR (240–280 nm). This demonstrates a higher kinetic rate of HONO photolysis on a per-photon (per-mJ) basis for shorter wavelength irradiation (240–280 nm) compared to broader UV-irradiation (240–400 nm) for the xenon lamp, enhanced by the photolysis of formic acid at short irradiation wavelengths [67]. Photocatalytic xenon lamp experiments with HONO used 1 g/L P90 and achieved 99.9% TNR (240–400 nm) and 84% TNR (240–280 nm). This increased HONO removal (10 times higher performance HONO:NO_2^-) corresponded to only a $1.6 \times$ higher molar

absorptivity in the ultraviolet wavelength range, further illustrating interplay of quantum yield (Φ) and molar absorptivity (ε). The quantum yield of the photolysis for HONO ($\Phi_{355nm} \approx 0.4$) is significantly higher when compared to nitrite ($\Phi_{355nm} = 0.025$) at 355 nm [53]. Acidification shifts nitrite speciation from NO_2^- to HONO; this greatly enhanced total nitrogen removal by increasing reaction rates and decreasing intermediate reaction steps [68,69]. Further, the shift in selectivity towards N-gases is mitigated by a primary intermediate of HONO reduction, HNO, which promotes terminal products of N-gases at acidic pH where aqueous N-intermediates are co-located at the photocatalyst surface [20].

On a photon fluence basis, higher aqueous nitrogen removal was observed with LED irradiation compared to the broad-spectrum xenon lamp. HONO (pH = 2.5) reduction using the 365 nm LED achieved > 93% TNR for photolysis (Fig. S1) and > 95% TNR with TiO_2 (Fig. S2). Negligible (< 5%) ammonium was produced under individual illumination with 285 nm or 300 nm LED and combined irradiation of 285 nm and 300 nm LEDs for both photolysis and photocatalysis. Complete reduction of HONO in solution with < 2% ammonium production was observed with 1.71×10^{19} photons/cm² at 365 nm. In contrast to the xenon lamp results, the LED light source (365 nm) showed no competitive advantage for nitrite reduction using TiO_2 (compared against direct photolysis) (Fig. 7). The high kinetic reduction of HONO observed was due to both the high absorbance and quantum yield of HONO and the absorption and scattering of light by TiO_2 at 365 nm. Further, the discrete wavelength irradiation (UV-LED) used only one-third of the photons (200 nm to 1100 nm) compared to the broad-spectrum (xenon) irradiation to achieve complete removal of HONO.

Selectivity of HONO reduction under photolytic and photocatalytic conditions with (1) single UV-LEDs (285 nm, 300 nm, or 365 nm) or (2) combinations thereof yielded > 88% and > 94% conversion to N-gases, respectively (Fig. S1, S2). For photocatalytic experiments, selectivity to undesired ammonium was always < 2%. Under illumination of a
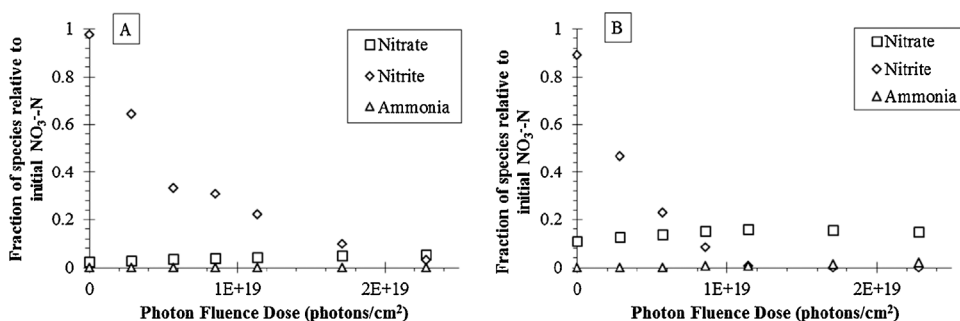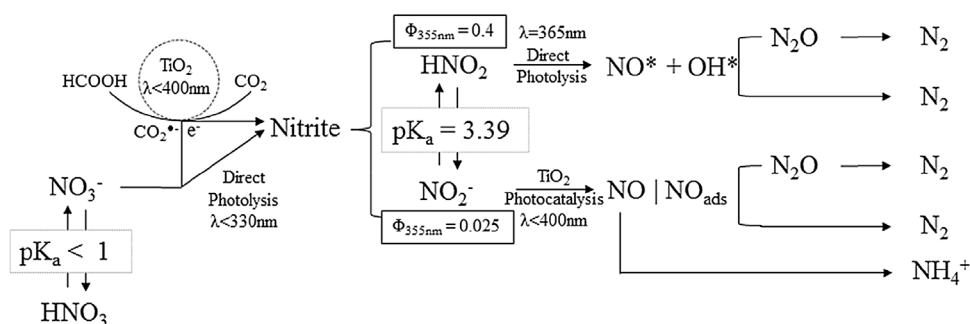

Fig. 7. Photolytic (A) and photocatalytic (B) nitrite reduction at 365 nm with formic acid (pH = 2.5) as a sacrificial hole scavenger. Photolytic experiments performed under UV-LED irradiation without TiO_2 and photocatalytic experiments were performed under UV-LED irradiation with 1 g/L P90.

combination of 285 nm and 300 nm irradiation, up to 100% selectivity to N-gases was achieved at > 97% photocatalytic reduction of HONO and 92.5% photolytic HONO reduction. HONO oxidation to nitrate was 4.6 ± 0.5% using a single 285 nm or 365 nm LED or a combination of 285, 300, and 365 nm irradiation for photocatalysis and increased to 6.0 ± 0.9% for photolysis across all wavelength combinations. Selectivity of aqueous ammonium in lieu of N-gases in photolytic experiments with UV-LEDs was ordered: $S_{300nm} > S_{285+300+365nm} > S_{365nm} > S_{285nm} > S_{285+300nm}$. These observations led to the understanding of wavelength influences for reaction kinetics, pathways and by-product selectivity as described in Scheme 2. Nitrate reduction via direct photolysis is thermodynamically feasible utilizing ultraviolet wavelengths [70], but it is not kinetically favorable for producing N-gases. This is due to the higher quantum yield of nitrite photolysis [53], which can be both reductive (N-gases/NH_4^+) [71] or oxidative (NO_3^-) [72]. Thermodynamically, conduction band electrons of TiO_2 are not sufficiently energetic to reduce nitrate to nitrite alone [5,73]. Hence, through the use of a hole scavenger such as formic acid, both a reduction in pH and production of radical species $CO_2 \cdot^-$, which can reduce nitrate [18], are achieved. As demonstrated in this work, both photolytic and photocatalytic pathways reduced nitrite/HONO to N-gases and aqueous ammonium. Key pathways may be enhanced by combining photocatalytic and photolytic processes with wavelengths targeted toward specific intermediates, e.g., NO/NO·, which have been previously demonstrated [69] to increase N-gases selectivity (Eqs. (11)–(16)). Further, pH is critical because many of the reactions require H^+ (Eqs. (4), (13), (16)), and HONO is significantly more photoactive than NO_2^-. Novel herein is the use of discrete wavelengths to demonstrate enhanced production of N-gases (Figs. 6, S1, S2, and Scheme 2).

4. Conclusions

Photocatalytic reduction of nitrate with TiO_2 progressed with varied kinetics and to different products based on applied wavelengths. Wavelengths of interest for nitrate reduction to N-gases were identified as 285 nm, 300 nm, and 365 nm to facilitate a combined outcome of photocatalytic and photolytic reduction. Further, selectivity of nitrate reduction toward semi-volatile versus soluble by-products can be managed via discrete wavelength light sources (e.g., LEDs), allowing for enhanced reductive performance on an energy- and photon-basis. Whereas photocatalysis is critical to nitrate reduction, protonated nitrite (HONO) is readily photolyzed between 350 and 370 nm with high Φ, which can explain high selectivity toward N-gases in previously reported medium and high pressure mercury lamp experiments [38] and the LED experiments in this work. HONO/HNO were proposed herein as the key intermediates for nitrate reduction to N-gases, which requires an acidic pH to selectively avoid ammonium production. Traditional irradiance sources (medium pressure mercury and xenon lamps) still provide higher photon flux to the solution than currently-available UV-LEDs, increasing temporal degradation kinetics but at significantly higher energetic and economic cost per mole of nitrate reduced (cost-

per-photon at 365 nm << cost-per-photon at 285 nm). Additionally, the efficiency of nitrate reduction via these lamps is diminished due to the ineffective photons produced in the visible and infrared regions, which cause increased temperature (controlled in these experiments) and decreased nitrate conversion performance. Polychromatic irradiance sources remain widely used due to their capacity for disinfection and higher output than low pressure mercury 253.7 nm monochromatic irradiance sources. As advanced UV-LEDs continue to come to market at lower cost and higher radiant intensity, their implementation in photocatalytic processes may be realized, particularly for small-systems water treatment.

Appendix A. Supplementary data

Supplementary data associated with this article can be found, in the online version, at http://dx.doi.org/10.1016/j.apcatb.2017.08.078.

References

[1] K.R. Burow, B.T. Nolan, M.G. Rupert, N.M. Dubrovsky, Nitrate in groundwater of the United States, 1991–2003, Environ. Sci. Technol. 44 (2010) 4988–4997, http://dx.doi.org/10.1021/es100546y.

[2] National Academy of Engineering, NAE Grand Challenges for Engineering, (2017).

[3] W.S.D. of Health, Nitrate Treatment: Alternatives for Small Water Systems, (2005).

[4] N. Wehbe, M. Jaafar, C. Guillard, J.-M. Herrmann, S. Miachon, E. Puzenat, et al., Comparative study of photocatalytic and non-photocatalytic reduction of nitrates in water, Appl. Catal. A Gen. 368 (2009) 1–8, http://dx.doi.org/10.1016/j.apcata.2009.07.038.

[5] J. Sá, C.A. Agüera, S. Gross, J.a. Anderson, Photocatalytic nitrate reduction over metal modified TiO2, Appl. Catal. B Environ. 85 (2009) 192–200, http://dx.doi.org/10.1016/j.apcatb.2008.07.014.

[6] U. Prüsse, M. Hähnlein, J. Daum, K.-D. Vorlop, Improving the catalytic nitrate reduction, Catal. Today 55 (2000) 79–90, http://dx.doi.org/10.1016/S0920-5861(99)00228-X.

[7] A. Pintar, Catalytic processes for the purification of drinking water and industrial effluents, Catal. Today 77 (2003) 451–465, http://dx.doi.org/10.1016/S0920-5861(02)00385-1.

[8] N. Barrabes, J. Sa, Catalytic nitrate removal from water, past, present and future perspectives, Appl. Catal. B Environ. 104 (2011) 1–5, http://dx.doi.org/10.1016/j.apcatb.2011.03.011.

[9] Y.X. Chen, Y. Zhang, G.H. Chen, Appropriate conditions or maximizing catalytic reduction efficiency of nitrate into nitrogen gas in groundwater, Water Res. 37 (2003) 2489–2495, http://dx.doi.org/10.1016/S0043-1354(03)00028-9.

[10] A.J. Lecloux, Chemical, biological and physical constrains in catalytic reduction processes for purification of drinking water, Catal. Today 53 (1999) 23–34, http://dx.doi.org/10.1016/S0920-5861(99)00100-5.

[11] R. Zhang, D. Shuai, K. a. Guy, J.R. Shapley, T.J. Strathmann, C.J. Werth, Elucidation

of nitrate reduction mechanisms on a Pd-in bimetallic catalyst using isotope labeled nitrogen species, ChemCatChem 5 (2013) 313–321, http://dx.doi.org/10.1002/cctc.201200457.

[12] W.T. Mook, M.H. Chakrabarti, M.K. Aroua, G.M. a Khan, B.S. Ali, M.S. Islam, et al., Removal of total ammonia nitrogen (TAN), nitrate and total organic carbon (TOC) from aquaculture wastewater using electrochemical technology: a review, Desalination 285 (2012) 1–13, http://dx.doi.org/10.1016/j.desal.2011.09.029.

[13] M. Safari, A. Rezaee, B. Ayati, A. Jonidi-Jafari, Simultaneous removal of nitrate and its intermediates by use of bipolar electrochemistry, Res. Chem. Intermed. 41 (2015) 1365–1372, http://dx.doi.org/10.1007/s11164-013-1279-9.

[14] C. Polatides, M. Dortsiou, G. Kyriacou, Electrochemical removal of nitrate ion from aqueous solution by pulsing potential electrolysis, Electrochim. Acta 50 (2005) 5237–5241, http://dx.doi.org/10.1016/j.electacta.2005.01.057.

[15] T. Yang, K. Doudrick, P. Westerhoff, Photocatalytic reduction of nitrate using titanium dioxide for regeneration of ion exchange brine, Water Res. 47 (2013) 1299–1307, http://dx.doi.org/10.1016/j.watres.2012.11.047.

[16] WHO, Nitrate and Nitrite in Drinking-Water, (2016).

[17] S. Gangolli, P. Van Den Brandt, V. Feron, C. Janzowsky, J. Koeman, G. Speijers, et al., Nitrate, nitrite and N-nitroso compounds, Eur. J. Pharmacol. 292 (1994) 1–38, http://dx.doi.org/10.1016/0926-6917(94)90022-1.

[18] V.N. Montesinos, N. Quici, H. Destaillats, M.I. Litter, Nitric oxide emission during the reductive heterogeneous photocatalysis of aqueous nitrate with TiO2, RSC Adv. 5 (2015) 85319–85322, http://dx.doi.org/10.1039/C5RA17914A.

[19] H. Kominami, A. Furusho, S. Murakami, H. Inoue, Effective photocatalytic reduction of nitrate to ammonia in an aqueous suspension of metal-loaded titanium (IV) oxide particles in the presence of oxalic acid, Catal. Lett. 76 (2001) 31–34, http://dx.doi.org/10.1023/A:1016771908609.

[20] H.O.N. Tugaoen, S. Garcia-Segura, K. Hristovski, P. Westerhoff, Challenges in the photocatalytic reduction of nitrate as a water treatment technology, Sci. Total Environ. 599–600 (2017) 1524–1551, http://dx.doi.org/10.1016/j.scitotenv.2017.04.238.

[21] K. Doudrick, T. Yang, K. Hristovski, P. Westerhoff, Photocatalytic nitrate reduction in water: managing the hole scavenger and reaction by-product selectivity, Appl. Catal. B Environ. 136–137 (2013) 40–47, http://dx.doi.org/10.1016/j.apcatb.2013.01.042.

[22] F. Zhang, R. Jin, J. Chen, C. Shao, W. Gao, L. Li, et al., High photocatalytic activity and selectivity for nitrogen in nitrate reduction on Ag/TiO2 catalyst with fine silver clusters, J. Catal. 232 (2005) 424–431, http://dx.doi.org/10.1016/j.jcat.2005.04.014.

[23] H. Kominami, T. Nakaseko, Y. Shimada, A. Furusho, H. Inoue, S.-Y. Murakami, et al., Selective photocatalytic reduction of nitrate to nitrogen molecules in an aqueous suspension of metal-loaded titanium(IV) oxide particles, Chem. Commun. 3 (2005) 2933–2935, http://dx.doi.org/10.1039/b502909k.

[24] Y.A. Shaban, A.A. El, R. Kh, A. Farawati, Journal of Photochemistry and Photocatalytic reduction of nitrate in seawater using C/TiO2 nanoparticles, J. Photochem. Photobiol. A Chem. 328 (2016) 114–121, http://dx.doi.org/10.1016/j.jphotochem.2016.05.018.

[25] G. Petriconi, H. Papee, Decomposition of sodium nitrate solutions under ultra-violet irradiation at 25 °C, J. Inorg. Nucl. Chem. 30 (1968) 1525–1535, http://dx.doi.org/10.1016/0022-1902(68)80292-1.

[26] H. Gekko, K. Hashimoto, H. Kominami, Photocatalytic reduction of nitrite to dinitrogen in aqueous suspensions of metal-loaded titanium(IV) oxide in the presence of a hole scavenger: an ensemble effect of silver and palladium co-catalysts, Phys. Chem. Chem. Phys. 14 (2012) 7965–7970, http://dx.doi.org/10.1039/c2cp40729a.

[27] M. Shand, J.A. Anderson, Aqueous phase photocatalytic nitrate destruction using titania based materials: routes to enhanced performance and prospects for visible light activation, Catal. Sci. Technol. 3 (2013) 879, http://dx.doi.org/10.1039/c3cy20851f.

[28] N. Lu, N.Y. Gao, Y. Deng, Q.S. Li, Nitrite formation during low pressure ultraviolet lamp irradiation of nitrate, Water Sci. Technol. 60 (2009) 1393–1400, http://dx.doi.org/10.2166/wst.2009.475.

[29] J. Yang, J. Dai, J. Li, Visible light induced photocatalytic removal of nitrate with Nd, n-codoped titania particles, Sci. Adv. Mater. 5 (2013) 1013–1023.

[30] K.T. Ranjit, B. Viswanathan, Photocatalytic reduction of nitrite and nitrate ions over doped TiO2 catalysts, J. Photochem. Photobiol. A Chem. 107 (1997) 215–220, http://dx.doi.org/10.1016/S1010-6030(97)00025-7.

[31] K.T. Ranjit, B. Viswanathan, Photocatalytic reduction of nitrite and nitrate ions to ammonia on M/TiO2 catalysts, J. Photochem. Photobiol. A Chem. 108 (1997) 73–78, http://dx.doi.org/10.1016/S1010-6030(96)04505-4.

[32] M. Penpolcharoen, R. Amal, M. Brungs, Degradation of sucrose and nitrate over titania coated nano-hematite photocatalysts, J. Nanopart. Res. 3 (2001) 289–302, http://dx.doi.org/10.1023/A:1017929204380.

[33] F. Zhang, Y. Pi, J. Cui, Y. Yang, X. Zhang, N. Guan, Unexpected selective photocatalytic reduction of nitrate to nitrogen on silver-doped titanium dioxide, J. Phys. Chem. C. 111 (2007) 3756–3761, http://dx.doi.org/10.1021/jp067807j.

[34] O. Hamanoi, A. Kudo, Reduction of nitrate and nitrite ions over Ni-ZnS photocatalyst under visible light irradiation in the presence of a sacrificial reagent, Chem. Lett. (2002) 838–839, http://dx.doi.org/10.1246/cl.2002.838.

[35] Y. Li, F. Wasgestian, Photocatalytic reduction of nitrate ions on TiO2 by oxalic acid, J. Photochem. Photobiol. A Chem. 112 (1998) 255–259, http://dx.doi.org/10.1016/S1010-6030(97)00293-1.

[36] B. Bems, F.C. Jentoft, R. Schlögl, Photoinduced decomposition of nitrate in drinking water in the presence of titania and humic acids, Appl. Catal. B Environ. 20 (1999) 155–163, http://dx.doi.org/10.1016/S0926-3373(98)00105-2.

[37] K.T. Ranjit, R. Krishnamoorthy, T.K. Varadarajan, B. Viswanathan, Photocatalytic reduction of nitrite on CdS, J. Photochem. Photobiol. A Chem. 86 (1995) 185–189,

http://dx.doi.org/10.1016/1010-6030(94)03930-S.

[38] K. Doudrick, O. Monzón, A. Mangonon, K. Hristovski, P. Westerhoff, Nitrate reduction in water using commercial titanium dioxide photocatalysts (P25, P90, and Hombikat UV100), J. Environ. Eng. 138 (2012) 852–861, http://dx.doi.org/10.1061/(ASCE)EE.1943-7870.0000529.

[39] L. Li, Z. Xu, F. Liu, Y. Shao, J. Wang, H. Wan, et al., Photocatalytic nitrate reduction over Pt-Cu/TiO2 catalysts with benzene as hole scavenger, J. Photochem. Photobiol. A Chem. 212 (2010) 113–121, http://dx.doi.org/10.1016/j.jphotochem.2010.04.003.

[40] R. Jin, W. Gao, J. Chen, H. Zeng, F. Zhang, Z. Liu, et al., Photocatalytic reduction of nitrate ion drinking water by using metal-loaded MgTiO3-TiO2 composite semiconductor catalyst, J. Photochem. Photobiol. A Chem. 162 (2004) 585–590, http://dx.doi.org/10.1016/S1010-6030(03)00420-9.

[41] W. Gao, R. Jin, J. Chen, X. Guan, H. Zeng, F. Zhang, et al., Titania-supported bimetallic catalysts for photocatalytic reduction of nitrate, Catal. Today 90 (2004) 331–336, http://dx.doi.org/10.1016/j.cattod.2004.04.043.

[42] O.S.G.P. Soares, M.F.R. Pereira, J.J.M. Órfão, J.L. Faria, C.G. Silva, Photocatalytic nitrate reduction over Pd–Cu/TiO2, Chem. Eng. J. 251 (2014) 123–130, http://dx.doi.org/10.1016/j.cej.2014.04.030.

[43] D. Sun, W. Yang, L. Zhou, W. Sun, Q. Li, J.K. Shang, The selective deposition of silver nanoparticles onto {101} facets of TiO2 nanocrystals with co-exposed {001}/{101} facets, and their enhanced photocatalytic reduction of aqueous nitrate under simulated solar illumination, Appl. Catal. B Environ. 182 (2016) 85–93, http://dx.doi.org/10.1016/j.apcatb.2015.09.005.

[44] A. Sowmya, S. Meenakshi, Photocatalytic reduction of nitrate over Ag-TiO2 in the presence of oxalic acid, J. Water Process Eng. 8 (2015) e23–e30, http://dx.doi.org/10.1016/j.jwpe.2014.11.004.

[45] K. Kobwittaya, S. Sirivithayapakorn, Photocatalytic reduction of nitrate over TiO2 and Ag-modified TiO2, J. Saudi Chem. Soc. 18 (2014) 291–298, http://dx.doi.org/10.1016/j.jscs.2014.02.001.

[46] H.T. Ren, S.Y. Jia, J.J. Zou, S.H. Wu, X. Han, A facile preparation of Ag2O/P25 photocatalyst for selective reduction of nitrate, Appl. Catal. B Environ. 176-177 (2015) 53–61, http://dx.doi.org/10.1016/j.apcatb.2015.03.038.

[47] G. Liu, S. You, H. Huang, N. Ren, Removal of nitrate by photocatalytic denitrification using nonlinear optical material, Environ. Sci. Technol. 50 (2016) 11218–11225, http://dx.doi.org/10.1021/acs.est.6b03455.

[48] S. Rengaraj, X.Z. Li, Enhanced photocatalytic reduction reaction over Bi3 + -TiO2 nanoparticles in presence of formic acid as a hole scavenger, Chemosphere 66 (2007) 930–938, http://dx.doi.org/10.1016/j.chemosphere.2006.06.007.

[49] I. Mora-Sero, T.L. Villarreal, J. Bisquert, Ä. Pitarch, R. Gomez, P. Salvador, Photoelectrochemical behavior of nanostructured TiO2 thin-Film electrodes in contact with aqueous electrolytes containing dissolved pollutants: a model for distinguishing between direct and indirect interfacial hole transfer from photocurrent measurement, J. Phys. Chem. B. 109 (2005) 3371–3380, http://dx.doi.org/10.1021/jp045585o.

[50] M. Fischer, P. Warneck, Photodecomposition of nitrite and undissociated nitrous acid in aqueous solution, J. Phys. Chem. 3654 (1996) 18749–18756, http://dx.doi.org/10.1021/jp961692 + .

[51] R. Zellner, M. Exner, H. Herrmann, Absolute OH quantum yields in the laser photolysis of nitrate, nitrite and dissolved H202 at 308 and 351 nm in the temperature range 278–353 K, J. Atmos. Chem. 10 (1990) 411–425, http://dx.doi.org/10.1007/BF00115783.

[52] O.C. Zafiriou, M.B. True, Nitrate photolysis in seawater by sunlight, Mar. Chem. 8 (1979) 33–42, http://dx.doi.org/10.1016/0304-4203(79)90030-6.

[53] J. Mack, J.R. Bolton, Photochemistry of nitrite and nitrate in aqueous solution: a review, J. Photochem. Photobiol. A Chem. 128 (1999) 1–13, http://dx.doi.org/10.1016/S1010-6030(99)00155-0.

[54] L. Chu, C. Anastasio, Quantum yields of hydroxyl radical and nitrogen dioxide from the photolysis of nitrate on ice, J. Phys. Chem. A 107 (2003) 9594–9602, http://dx.doi.org/10.1021/jp0349132.

[55] V.N. Montesinos, N. Quici, H. Destaillats, M.I. Litter, Nitric oxide emission during the reductive heterogeneous photocatalysis of aqueous nitrate with TiO 2, RSC Adv. 5 (2015) 85319–85322, http://dx.doi.org/10.1039/C5RA17914A.

[56] H. Kominami, H. Gekko, K. Hashimoto, Photocatalytic disproportionation of nitrite to dinitrogen and nitrate in an aqueous suspension of metal-loaded titanium(IV) oxide nanoparticles, Phys. Chem. Chem. Phys. 12 (2010) 15423–15427, http://dx.doi.org/10.1039/c0cp00794c.

[57] H. Kato, A. Kudo, Photocatalytic reduction of nitrate ions over tantalate photocatalysts, Phys. Chem. Chem. Phys. 4 (2002) 2833–2838, http://dx.doi.org/10.1039/b110511f.

[58] M. Stefan, J. Bolton, Fundamental approach to the fluence-based kinetic and electrical energy efficiency parameters in photochemical degradation reactions: polychromatic light, J. Environ. Eng. 18 (2005) 13–18, http://dx.doi.org/10.1139/S04-026.

[59] J. Bolton, M. Stefan, Fundamental photochemical approach to the concepts of fluence (UV dose) and electrical energy efficiency in photochemical degradation reactions, Res. Chem. Intermed. 28 (2002) 857–870, http://dx.doi.org/10.1163/15685670260469474.

[60] J.R. Bolton, K.G. Linden, Standardization of methods for fluence (UV dose) determination in bench-scale UV experiments, J. Environ. Eng. 129 (2003) 209–215, http://dx.doi.org/10.1061/(ASCE)0733-9372(2003)129:3(209).

[61] K.G. Linden, J.L. Darby, Estimating effective germicidal dose from medium pressure UV lamps, J. Environ. Eng. 123 (1997) 1142–1149, http://dx.doi.org/10.1061/(ASCE)0733-9372(1997)123:11(1142).

[62] S.E. Beck, H. Ryu, L.A. Boczek, J.L. Cashdollar, K.M. Jeanis, J.S. Rosenblum, et al., Evaluating UV-C LED disinfection performance and investigating potential dual-

wavelength synergy, Water Res. 109 (2017) 207–216, http://dx.doi.org/10.1016/j.watres.2016.11.024.

[63] F. Barat, L. Gilles, B. Hickel, Sutton, flash photolysis of the nitrate ion in aqueous solution: excitation at 200 nm, J. Chem. Soc. A Inorg. Phys. Theor. (1970) 1982–1986, http://dx.doi.org/10.1039/J19700001982.

[64] M.C. Gonzalez, A.M. Braun, VUV photolysis of aqueous solutions of nitrate and nitrite, Res. Chem. Intermed. 21 (1995) 837–859, http://dx.doi.org/10.1163/156856795x00512.

[65] N.K. Scharko, A.E. Berke, J.D. Raff, Release of nitrous acid and nitrogen dioxide from nitrate photolysis in acidic aqueous solutions, Environ. Sci. Technol. 48 (2014) 11991–12001, http://dx.doi.org/10.1021/es503088x.

[66] M. Shand, J.a. Anderson, Aqueous phase photocatalytic nitrate destruction using titania based materials: routes to enhanced performance and prospects for visible light activation, Catal. Sci. Technol. 3 (2013) 879, http://dx.doi.org/10.1039/c3cy20851f.

[67] F. Crapulli, D. Santoro, M.R. Sasges, A.K. Ray, Mechanistic modeling of vacuum UV advanced oxidation process in an annular photoreactor, Water Res. 64 (2014) 209–225, http://dx.doi.org/10.1016/j.watres.2014.06.048.

[68] S. Goldstein, D. Behar, T. Rajh, J. Rabani, Nitrite reduction to nitrous oxide and ammonia by TiO 2 electrons in a colloid solution via consecutive one-electron

transfer reactions, J. Phys. Chem. A 120 (2016) 2307–2312, http://dx.doi.org/10.1021/acs.jpca.6b01761.

[69] A. Hérissan, J.M. Meichtry, H. Remita, C. Colbeau-justin, M.I. Litter, Reduction of nitrate by heterogeneous photocatalysis over pure and radiolytically modified TiO2 samples in the presence of formic acid, Catal. Today 281 (2017) 101–108, http://dx.doi.org/10.1016/j.cattod.2016.05.044.

[70] S. Goldstein, J. Rabani, Mechanism of nitrite formation by nitrate photolysis in aqueous solutions: the role of peroxynitrite, nitrogen dioxide, and hydroxyl radical, J. Am. Chem. Soc. 129 (2007) 10597–10601, http://dx.doi.org/10.1021/ja073609+.

[71] A. Treinin, E. Hayon, Absorption spectra and reaction kinetics of NO2, N2O3, and N2O4 in aqueous solution, J. Am. Chem. Soc. 92 (1970) 5821–5828, http://dx.doi.org/10.1021/ja00723a001.

[72] G. Mark, H.G. Korth, H.P. Schuchmann, C. Von Sonntag, The photochemistry of aqueous nitrate ion revisited, J. Photochem. Photobiol. A Chem. 101 (1996) 89–103, http://dx.doi.org/10.1016/S1010-6030(96)04391-2.

[73] A.R. Cook, N. Dimitrijevic, B.W. Dreyfus, D. Meisel, L.A. Curtiss, D.M. Camaioni, Reducing radicals in nitrate solutions. the NO32 – system revisited, J. Phys. Chem. A 105 (2001) 3658–3666, http://dx.doi.org/10.1021/jp0038052.